OXFORD GENETICS

GENETICS, 2023, 225(3), iyad167
https://doi.org/10.1093/genetics/iyad167
Advance Access Publication Date: 15 September 2023
Investigation

Identification of CryAB as a target of NUAK kinase activity in *Drosophila* muscle tissue

Ziwei Zhao, David Brooks, Yungui Guo, Erika R. Geisbrecht*

Department of Biochemistry and Molecular Biophysics, Kansas State University, 1711 Claflin Rd, Manhattan, KS 66506, USA

*Corresponding author: Department of Biochemistry and Molecular Biophysics, Kansas State University, 1711 Claflin Rd, Manhattan, KS 66506, USA. Email: geisbrechte@ksu.edu

Phosphorylation reactions performed by protein kinases are one of the most studied post-translational modifications within cells. Much is understood about conserved residues within protein kinase domains that perform catalysis of the phosphotransfer reaction, yet the identity of the target substrates and downstream biological effects vary widely among cells, tissues, and organisms. Here, we characterize key residues essential for NUAK kinase activity in *Drosophila melanogaster* myogenesis and homeostasis. Creation of a *NUAK* kinase-dead mutation using Clustered Regularly Interspaced Short Palindromic Repeats (CRISPR)/Cas9 results in lethality at the embryo to larval transition, while loss of NUAK catalytic function later in development produces aggregation of the chaperone protein αB-crystallin/CryAB in muscle tissue. Yeast 2-hybrid assays demonstrate a physical interaction between NUAK and CryAB. We further show that a phosphomimetic version of NUAK promotes the phosphorylation of CryAB and this post-translational modification occurs at 2 previously unidentified phosphosites that are conserved in the primary sequence of human CryAB. Mutation of these serine residues in *D. melanogaster* NUAK abolishes CryAB phosphorylation, thus, proving their necessity at the biochemical level. These studies together highlight the importance of kinase activity regulation and provide a platform to further explore muscle tissue proteostasis.

Keywords: muscle; NUAK; CryAB; *Drosophila*

Introduction

Protein kinases have broad functions in regulating molecular aspects of cell signaling as well as imparting diverse outputs in biological processes. While many substrates of kinase activity have been identified, there are 100s of kinase-substrate pairs still waiting to be uncovered. Since the deregulation of kinase activity leads to cancer and other diseases, dissecting kinase-substrate relationships is of great importance for the development of therapeutic targets. However, it is difficult to predict or extrapolate generalized phosphorylation events as many kinases are activated in response to varied extracellular insults and/or have tissue-specific targets.

Multiple approaches, each with its own advantages and limitations, exist to identify and verify protein kinase substrates (Xue and Tao 2013). Genetic screens can be performed to uncover candidate substrates that mimic and/or modify kinase mutant phenotypes. While genetic methods will identify kinase-substrate pairs that are physiologically or functionally relevant, these experiments must be followed up with biochemical verification. High throughput methods include peptide arrays, phage display, or mass spectrometry (MS)-based phosphoproteomic profiling (Dente *et al.* 1997; Chen and Turk 2010; Breitkopf and Asara 2012). Alternatively, computational approaches to predict phosphorylation motifs in addition to protein interaction-based screens such as yeast 2-hybrid (Y2H) or affinity purification have been successfully utilized to uncover kinase substrates (Xue and Tao 2013). The gold standard for kinase-substrate verification is the in vitro kinase assay, whereby purified kinase is incubated with candidate substrate in the presence of ATP to detect phosphotransfer activity (Hastie *et al.* 2006; Li *et al.* 2008). Ultimately, all of these lines of inquiry are necessary to uncover and validate kinase-substrate pairs.

AMP-activated protein kinase (AMPK) is a phylogenetically conserved serine/threonine (S/T) kinase that senses cellular ATP levels and redirects metabolism based on energy requirements (Hardie 2011; Herzig and Shaw 2018; Steinberg and Hardie 2023). Twelve additional AMPK-related protein kinases [NUAK family kinase 1 (NUAK1/2), BR serine/threonine kinase 1 (BRSK1/2), Salt-inducible kinase (SIK1/2/3), MAP/microtubule affinity-regulating kinase (MARK1/2/3/4), and Maternal embryonic leucine zipper kinase (MELK)] have been identified that share extensive sequence homology with the catalytic kinase domain of AMPK, yet lack the regulatory subunits that mediate energy homeostasis (Bright *et al.* 2009; Sun *et al.* 2013). Phosphorylation of a conserved threonine in the T-loop region in the kinase domain of all AMPK-related protein kinases promotes activation of downstream physiological processes. With the exception of MELK, this phosphorylation can be mediated by Liver kinase B1 (LKB1) (Lizcano *et al.* 2004; Alessi *et al.* 2006) or a handful of other kinases, although this regulation may be protein or context-dependent (Bright *et al.* 2009).

Mammalian NUAK1/AMPK-related protein kinase 5 (ARK5) and NUAK2/SNF1/AMP kinase-related kinase (SNARK) can impact cytoskeletal rearrangement, insulin signaling, cell death, and cancer migration and metastasis (Sun *et al.* 2013; Bennison *et al.* 2022). Based on published literature and expression databases (https://www.proteinatlas.org/), both NUAK1 and NUAK2 show overlapping mRNA expression in multiple tissues (Sun *et al.* 2013; Molina *et al.* 2021; Bennison *et al.* 2022). However, *NUAK1 mRNA* is more highly enriched in the brain and muscle, while *NUAK2*

Received on 28 June 2023; accepted on 30 August 2023

mRNA is more predominant in the gastrointestinal tract and blood cells. Thus, expression alone does not provide insight into unique or redundant functions of NUAK1 or NUAK2. While TGF-β transcriptionally induces both *NUAK1* and *NUAK2* expression, each has opposing roles in outputs of this signaling pathway (van de Vis *et al.* 2021). Independent roles for both proteins have been identified in skeletal muscle, whereby NUAK1 suppresses insulin-mediated glucose uptake and NUAK2 regulates contraction-stimulated glucose transport (Koh *et al.* 2010; Inazuka *et al.* 2012). These biological differences may be mediated by distinct phosphorylation events.

A handful of NUAK1 and/or NUAK2 kinase targets have been uncovered in various cell types, each with diverse downstream consequences. Shared substrates of both NUAK1 and NUAK2 kinase activity include Large tumor suppressor kinase 1 (LATS1) in human embryonic kidney (HEK) 293 cells and the Protein phosphatase 1 (PP1) subunit myosin phosphatase targeting protein (MYPT) in multiple cell types (Yamamoto *et al.* 2008; Zagórska *et al.* 2010; Bonnard *et al.* 2020). Ataxia telangiectasia-mutated (ATM) and p53 are additional target substrates of NUAK1 upon glucose starvation, among others (Suzuki *et al.* 2003; Hou *et al.* 2011). Despite this knowledge, many targets of NUAK activity remain to be identified.

Our lab has focused on deciphering the biological roles of the *D. melanogaster* ortholog of mammalian NUAK1/2 (Brooks *et al.* 2020, 2022). Relevant to this manuscript, *NUAK* mutants exhibit progressive muscle degeneration concomitant with the impairment of autophagy (Brooks *et al.* 2020). In this study, we further examined candidates that arose from a Y2H screen using NUAK as a bait protein and identified αB-crystallin, or CryAB/l(2)efl. We further show that NUAK kinase activity promotes CryAB phosphorylation and is essential to prevent CryAB accumulation in muscle tissue. Together, these data expand the spectrum of NUAK kinase targets and provide a molecular role for NUAK in the regulation of CryAB function.

Materials and methods

Drosophila stocks and husbandry

All stocks were reared at 25°C on standard cornmeal-molasses-yeast media. w^{1118} was used as the *WT* control with the inclusion of *Canton-S* in Fig. 1c. The $NUAK^{R829}$ mutants and sls-GFP insertion ($sls^{ZCL2144}$) were previously published (Hudson *et al.* 2008; Brooks *et al.* 2020). *Drosophila* stocks obtained from the Bloomington (BL) *Drosophila* Stock Center (BDSC) are indicated with BL followed by the stock number. The following Gal4 drivers were used to direct expression in muscle tissue: *Mef2*-Gal4 (BL27390), *C57*-Gal4 (L. Wallrath), and *G7*-Gal4 (M. Baylies). Muscle phenotypes due to induction of UAS-*NUAK RNAi* (BL31885) and the generation of NUAK transgenes (UAS-*NUAK FL 548*, UAS-*NUAK K99R*, and UAS-*NUAK E197K*) were described previously (Brooks *et al.* 2020). UAS-*lacZ* (BL3956) was used as a control for Gal4-mediated experiments and UAS-*mCherry.NLS* (BL38424) was utilized to confirm the lack of *G7* expression in embryonic muscles. The UAS-*CryAB-3xHA* stock (F003130) was obtained from the FlyORF project (Bischof *et al.* 2013) and UAS-*CryAB RNAi* (BL41724) was used to confirm anti-CryAB specificity. See a list of all stocks and reagents in Supplementary Table 1.

CRISPR/Cas9 NUAK allele

CRISPR-mediated mutagenesis was performed by WellGenetics Inc. using modified methods of Kondo and Ueda (Kondo and Ueda 2013). In brief, the gRNA sequences CATCAAGAAGTGCAAGATCG[AGG]/TCATAATCTGCACCTCGCGA[CGG] were cloned into the U6 promoter plasmid separately. The K99R-BacDsRed cassette containing 2 PBac terminals, 3 × P3-DsRed, and 2 homology arms with the point mutation K99R were cloned into pUC57 Kan as a donor template for repair. NUAK/CG43143 targeting gRNAs and hs-Cas9 were supplied in DNA plasmids, together with a donor plasmid for microinjection into embryos of control strain w^{1118}; *attP40[nos Cas9]/CyO*. F1 flies carrying the 3xP3-DsRed selection marker were further validated by genomic PCR and sequencing for the introduction of the K99R point mutation. The DsRed selection marker was excised and we again reconfirmed the K99R mutation using PCR amplification followed by sequencing (Genewiz, South Plainfield, NJ). Primer sequences were forward 5′-ATGGTGATAAGCAAACCCGATGG AGC-3′ and reverse 5′- GATCTTGTGCTTGTGACAGTAGTAGA-3′.

Quantitative RT-PCR

RNA was extracted from 10 dissected L3 muscle carcasses for each genotype using the RNAeasy Mini Kit (Qiagen, Valencia, CA). Following elution from the column, RNA concentrations were measured and single-strand complementary DNA (cDNA) was generated from 175 ng of RNA using the SuperScript VILO cDNA Synthesis Kit (Invitrogen, Carlsbad, CA). For each qPCR reaction, the cDNA sample was diluted to 1:25 and mixed with PowerUp™ SYBR™ Green Master mix and primers (Applied Biosystems, Foster City, CA). *rp49* was the reference gene. Integrated DNA Technologies (IDT) synthesized the following primers: *rp49* forward 5′-GCCCAAGGGTAT CGACAACA-3′, *rp49* reverse 5′-GCGCTTGTT CGATCCGTAAC-3′; *NUAK* forward 5′-ATGGTGATAAGCAAACCCG ATGGAACG-3′, reverse 5′-GATCTTGTGCTTGTGACAGTAGTAGA-3′; and *l(2)efl/CryAB* forward 5′-TTCCACCCTCAACATCGACA, reverse 5′-CATGCTTTCCCTCCACGATG. Three independent biological replicates were processed for each genotype and reactions were run in triplicate using the Quant Studio 3 Applied Biosystem with Quant Studio design and analysis software. The average of the triplicates was used to calculate the 2-ΔΔCt values (normalized fold expression). Quantification of mRNA levels between genotypes was performed using the student *t*-test.

Creation of transgenic flies

NUAK

The QuikChange II XL Site-directed Mutagenesis kit (Agilent Technologies, Santa Clara, CA) was used to introduce the T226A mutation into the *NUAK-RD* cDNA in the pENTR™/D-TOPO vector (ThermoFisher Scientific, Waltham, MA). Primers used were forward 5′- GAACCGCAAAAGGCGCCCAGCAGTCGC-3′ and reverse 5′-GCGACTGCTGGGCGCCTTTTGCGGTTC-3′. The resulting mutagenized sequence was recombined into the pTW (pUAS without tag) destination plasmid to generate UAS-*NUAK T226A* using standard Gateway cloning protocols (Reece-Hoyes and Walhout 2018). All other UAS-*NUAK* lines (*DsNUAK T226E*, *HsNUAK1*, *HsNUAK1 K84R*, *HsNUAK2*, and *HsNUAK2 K81R*) were created using gene synthesis by Genscript and subcloned into the upstream activating sequence (pUAST) vector using NotI and XbaI restriction sites. Plasmid DNA from all constructs was purified with a Qiagen Maxi Kit (Hilden, Germany), sequence verified, and sent to Rainbow Trangenics for the creation of transgenic flies. The insertions were balanced on their respective chromosomes.

CryAB

cDNA corresponding to the coding region of *CryAB-RC* was synthesized by Genscript and subcloned into the pUASTattB vector using EcoRI/XbaI sites. All phosphosite mutations were performed by

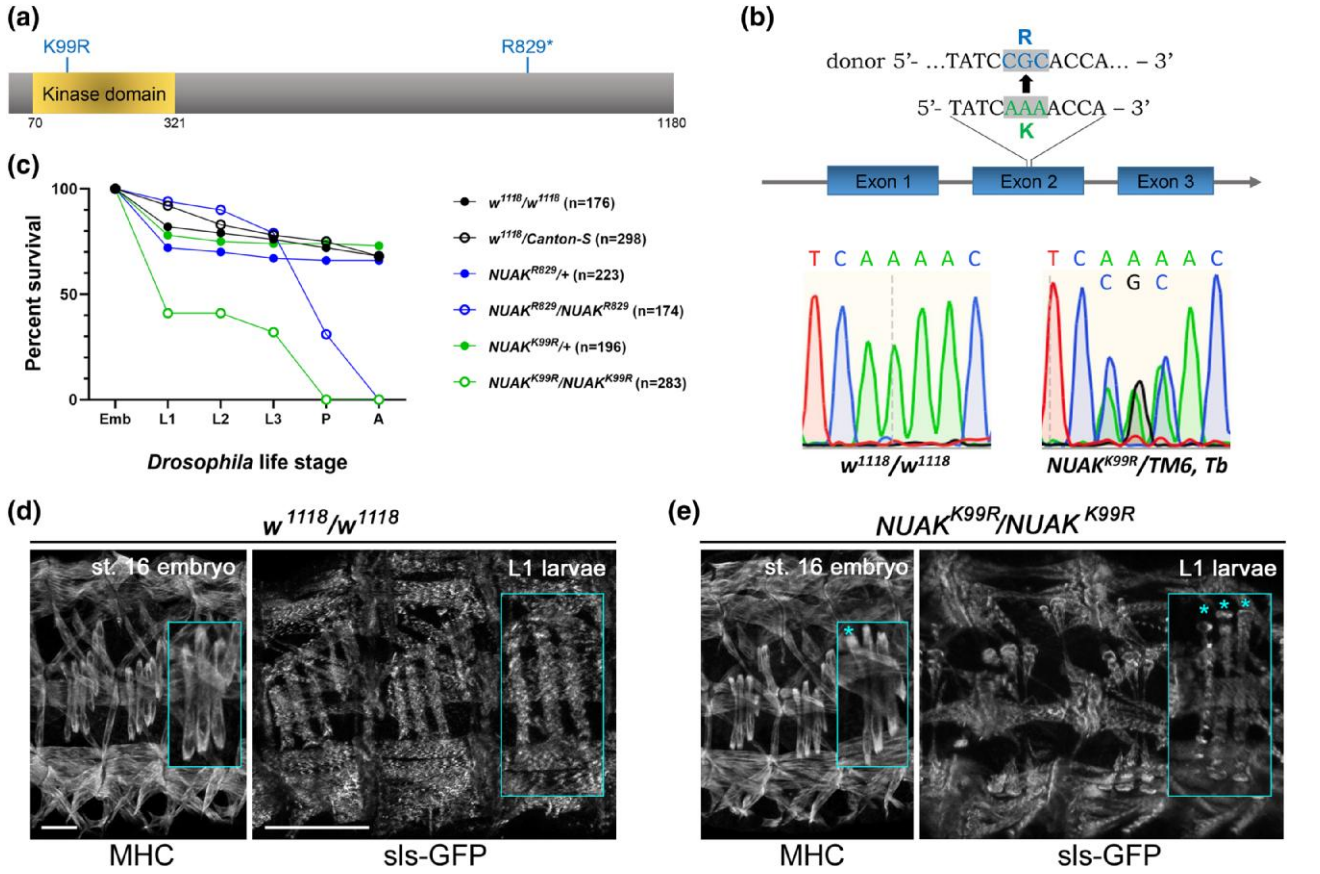

Fig. 1. A kinase-dead mutation in NUAK causes early lethality. a) Schematic of the *D. melanogaster* NUAK protein isoform PD showing the conserved kinase domain spanning AA 70-321. The location of the K99R and R829* alleles are shown. b) Sequence verification of the K→R change at residue 99 in $NUAK^{K99R}$/+ flies. The top panel shows WT and donor sequences. Sanger sequencing chromatogram of WT or $NUAK^{K99R}$/+ flies verify the desired nucleotide change. c) Lethal phase of *NUAK* mutants. Either *WT* or *NUAK* heterozygous controls largely survive until adulthood. Homozygous $NUAK^{R829*}/NUAK^{R829*}$ individuals are lethal at the pupal stage, while more than 50% of the $NUAK^{K99R}/NUAK^{K99R}$ mutants die at the embryo/L1 transition. *Drosophila* life cycle stage abbreviations—Emb, Embryo; L1, first larval stage; L2, second larval stage; L3, third larval stage; P, pupal stage; A, adult. d and e) Stage 16 embryos stained with anti-MHC (left panel) or L1 muscles marked with sls-GFP (right panel). The third set of lateral transverse muscles is enlarged in each panel (inset). d) Three hemisegments of the *WT* embryonic musculature adopt a stereotypical organization. This muscle pattern is preserved in L1 muscles and sarcomeres are marked by sls-GFP labeled Z-discs. e) Embryos homozygous mutant for the $NUAK^{K99R}$ allele exhibits an overall normal muscle pattern, although some muscles appear thinner (*). This thinning phenotype is exacerbated in L1 muscles. Emb scale bar, 20 μm. L1 scale bar, 50 μm.

Genscript to produce UAS-*CryAB S68A*, UAS-*CryAB S68E*, UAS-*CryAB S70A*, UAS-*CryAB S70E*, and UAS-*CryAB S68/70A*. Plasmid DNA was purified using the Qiagen Maxi kit (Hilden, Germany) and sent to Rainbow Trangenics. After generation of transgenic flies at the PhiC31 landing site (BL9736-53B2), all lines were balanced over the Cyo, Tb balancer (BL36335).

Visualization of muscle tissue

Embryo immunostaining

Crosses of the desired genotypes were set up in FlyStuff embryo collection cages (#59-105; Genesee Scientific, San Diego, CA) and inverted onto 35 mm Petri dishes containing apple juice-agar with fresh yeast paste. The pots were placed in an incubator at 25°C and 60% humidity where flies were allowed to lay eggs. After 2–3 hours, the collection plate was further staged for ~15 hours and a new plate was used to collect the next batch of embryos. Using a wet paintbrush, the embryos were collected into a mesh basket filled with 1× PBS and rinsed to remove yeast paste. Embryos were dechorionated in freshly diluted 50% bleach and rinsed with a solution of 0.7% NaCl/0.04% Triton X-100 before transferring to small glass vial containing a 1:1 fixative solution of heptane and 4% formaldehyde in PEM buffer (0.1 M Pipes, pH 8.0; 2 mM $MgSO_4$; 1 mM EGTA). The embryos were shaken vigorously for 12 minutes on a platform shaker to ensure penetration of the fixative solution. The bottom layer of fixative was removed and an equal volume of methanol was added. The settled embryos were transferred to a microcentrifuge tube, and washed 3 times with methanol, followed by 3 washes with Phosphate-buffered saline + 0.1% Tween 20 (PBT). Embryos were blocked in PBT with 5% normal goat serum for 30 min before incubating in mouse anti-Myosin heavy chain (Mhc) (1:100; Susan Abmayr) or rat anti-Tropomyosin (TM) MAC141 (1:50; Babraham Institute, Cambridge, UK) in PBT and 5% normal goat serum at 4°C overnight or at room temperature for 2 hours. Embryos were washed three times for 10 minutes each in PBT and reblocked in PBT with 5% normal goat serum for 30 minutes. Fluorescent antimouse Alexa Fluor 488 or antirat Alexa Fluor 488 (1:400, ThermoFisher Scientific, Waltham, MA) were added for 1 hour at room temperature. The embryos were again washed three times for 10 minutes each in PBT. After washing, the embryos were mounted onto glass slides, and imaged with a Zeiss 700.

Larval muscle staining

Wandering L3 larvae for the indicated genotypes were raised at 31°C, heat-killed, placed onto a Sylgard plate, pinned near the

mouth hooks at the anterior end and the internal organs were removed. The muscle carcasses were fixed in 4% formaldehyde and immunostained using standard immunostaining protocols, with normal goat serum used as a blocking agent in PBT. Tissues were stained with the following primary antibodies: rabbit anti-CryAB DZ33926 (1:200, Boster Bio, Pleasanton, CA) or mouse anti-Prm 5-23 [1:200, Developmental Studies Hybridoma Bank (DSHB)]. Secondary antibodies were used to detect fluorescence: antirabbit or antimouse Alexa Fluor 488 or 594 (1:400, Invitrogen, Waltham, MA). Phalloidin 594 was used to label F-actin (1:400, Molecular Probes, Eugene, OR). A Zeiss 700 confocal microscope was used to capture the images.

Live imaging

A small square of biofoil (AB-0718, Thermo Scientific) was cut and placed on the center of a glass slide in preparation for imaging. Using a wet paintbrush, an embryo of the appropriate developmental stage was immersed in halocarbon oil (#27 sigma) before transferring to the biofoil and orienting it properly for imaging. A coverslip was added over the embryo with small pieces of clay at the corners for support. Live imaging was performed with a Zeiss 700 using the following parameters: 20× objective, 1× zoom; time interval: 10 min; total time: 4 hours; laser power: 1.

Image processing

Image processing and analysis were performed using a combination of Zen Black (Zeiss), ImageJ (NIH), and Adobe Photoshop. All images taken at 20× are displayed as maximum intensity projections. Data acquisition at increased magnifications (63×) is presented as single-plane images.

Western blotting

Larvae for Western blots were raised at 31°C and dissected muscle carcasses were placed into 3× SDS sample buffer [188 mM Tris–HCl (pH 6.8), 3% (w/v) SDS, 30% (v/v) glycerol, 0.01% (w/v) bromophenol-blue, and 15% (v/v) β-mercaptoethanol], boiled at 95°C for 3 min, homogenized, boiled for an additional 10 min at 95°C, and centrifuged at 20,000×g for 1 min to pellet debris. The resulting protein samples were separated by sodium dodecyl sulfate-polyacrylamide gel electrophoresis (SDS-PAGE) and transferred to the nitrocellulose blotting membrane (pore size 0.45 μm, Cytiva, Marlborough, MA) using the Trans-Blot Turbo Transfer System (Bio-Rad, Hercules, CA). Membranes were probed with the following primary antibodies: rabbit anti-l(2)efl/CryAB DZ33926 (1:1000, Boster Bio, Pleasanton, CA), rabbit anti-NUAK DZ41105 (1:400, Boster Bio, Pleasanton, CA), rabbit anti-pT211 AB-PK737 (1:1000, Kinexus, Vancouver, Canada), mouse anti-ATP5α ab14748 (1:20000, Abcam, Waltham, MA). IRDye 800CW antirabbit and IRDye 680RD antimouse secondary antibodies (LI-COR Biosciences, Lincoln, NE) were used at 1:10,000 and Revert 700 Total Protein Stain (LI-COR Biosciences, Lincoln, NE) or anti-ATP5α was used as a loading control. Membranes were developed using the LI-COR Odyssey XF and quantitation of relative protein levels was performed in Empiria Studio Software (LI-COR Biosciences, Lincoln, NE).

Lambda protein phosphatase treatment

Three dissected *Mef2* > *NUAK OE* larvae reared at 25°C were dissected and lysed into 100 μL Protein MetalloPhosphatases (PMP) buffer with a pestle. The resulting lysates were spun down at 13,000×g at 4°C for 10 min. The samples were split into untreated (45 μL, 5 μL $MnCl_2$, 1 μL ultrapure water) and treated (45 μL, 5 μL $MnCl_2$, 1 μL lambda-phosphatase P0753S) (New England Biolabs, Ipswich, MA) groups. Both samples were incubated for 1 hr at 30°C followed by overnight at room temperature. After incubation, 50 μL of 3× SDS sample buffer was added before boiling and SDS-PAGE as described above.

Yeast 2-hybrid (Y2H)

Y2H assays were carried out by Hybrigenics Services (Gard, FR). The coding sequence of the full-length *D. melanogaster* NUAK/CG43143 (GenBank accession number NM_206469.3) was PCR-amplified and cloned in frame with the Gal4 DNA binding domain (DBD) into plasmid pB66 as a C-terminal fusion to Gal4 (Gal4-bait fusion). Prey fragments of Prm (AA 588-867) or CryAB (AA 78-156) corresponding to the smallest region that interacts with NUAK were cloned in-frame with the Gal4 activation domain (AD) into plasmid pP6. Bait and prey constructs were transformed in the yeast haploid cells CG1945 (mata) and YHGX13 (Y187ade2-101::loxP-kanMX-loxP, matα) and diploid yeast cells were obtained using a mating protocol with both yeast strains. The interaction between Mothers against decapentaplegic (SMAD) and E3 ubiquitin-protein ligase SMURF (SMURF) is used as a positive control (Colland *et al.* 2004). As negative controls, all prey plasmids were tested with the empty bait vector pB66. Streaks were plated for three independent yeast clones for each control and interaction. Medium lacking tryptophan and leucine were used as a growth control and to verify the presence of the bait and prey plasmids. The selective medium without tryptophan, leucine, and histidine was used to confirm the interaction between bait and prey.

Lethal stage analysis

For each of the analyzed genotypes, 50 embryos/replicates were placed in a grid pattern on apple juice-agar plates with yeast paste at 25°C. Embryos that hatched were transferred onto new apple juice-agar plates supplemented with yeast paste and analyzed at ~24 hr intervals for lethality or transferred to new plates. The number of dead, missing, or living individuals was counted and recorded for each stage. The survival plot curve in Prism was used to display the data. $N \geq 3$ biological replicates.

Proximity ligation assay

Wandering L3 larvae raised at 25°C of the genotypes *Mef2* > *lacZ*, *Mef2* > *CryAB::3xHA*, or *Mef2* > *NUAK OE; CryAB-3xHA* were heat-killed, dissected, fixed in 4% formaldehyde and washed in PBT before following instructions for the Duolink In Situ Red Starter Kit Mouse/Rabbit (Sigma-Aldrich, St. Louis, MO). Tissues were blocked for 1 h at 37°C in the Duolink blocking solution, incubated with primary antibody diluted in the Duolink antibody diluent overnight at 4°C. Primary antibodies used were mouse anti-HA 6E2 (1:400, Cell Signaling Technology, Danvers, MA); anti-NUAK DZ41105 (1:400, Boster Bio, Pleasanton, CA). Tissues were washed twice for 5 min in wash buffer A and then incubated in 40 μL proximity ligation assay (PLA) probe solution (8 μL PLUS probe, 8 μL MINUS probe, 24 μL antibody diluent) for 1 h at 37°C. Tissues were washed twice for 5 min in wash buffer A and then incubated for 30 min at 37°C in 40 μL ligation solution (8 μL ligation buffer, 31 μL ddH_2O, 1 μL ligase). Tissues were again washed twice for 5 min in wash buffer A and incubated for 100 min at 37°C in 40 μL amplification solution (8 μL amplification buffer, 31.5 μL ddH_2O, 0.5 μL polymerase). Tissues were washed twice for 10 min in wash buffer B, then rinsed for 1 min with 0.01× wash buffer B and Phalloidin 488 to label F-actin (1:400, Molecular Probes, Eugene, OR). Tissues were mounted in PLA mounting medium.

Determination of CryAB phosphosites

Wandering L3 larvae of the genotype *Mef2* > *NUAK OE; CryAB::3xHA* were used for the determination of phosphorylated residues via MS. Larvae were raised in cages at 31°C and rinsed with Phosphate-buffered saline (PBS). Larvae equivalent to ~3 mL volume were transferred into a 15 mL Dounce tissue grinder (Wheaton, USA) with 2 mL lysis buffer (50 mM Tris–HCl pH 7.5, 150 mM NaCl, 1% Triton X-100, 10% glycerol) plus inhibitors (1 × Halt protease inhibitor cocktail, 1 × Halt phosphatase inhibitor cocktail; 1 mM Na_3VO_4, 1 mM NaF, 1 mM PMSF, 10 μM MG132, 0.001% PTU, 5 mM α-Naphthyl acid phosphate monopotassium salt). The lysates were spun at 15,000 rpm for 10 min at 4°C to harvest the supernatant. The resulting lysate was incubated with pre-washed (in 0.05% TBS-T buffer) Pierce anti-HA conjugated magnetic beads #88837 (ThermoFisher Scientific, Waltham, MA) for 2 hours at room temperature. The beads with bound proteins were washed twice with 0.05% TBS-T and eluted with SDS sample buffer. Samples were boiled at 95°C for 10 mins before running on a 15% SDS-page gel. After Coomassie blue staining, bands corresponding to the predicted molecular weight of CryAB-3xHA were cut out of the gel, placed into a sterile 1.5 mL microcentrifuge tube, and sent to the Taplin Biological MS Facility at Harvard University for phosphosite identification.

Protein structure overlay

The Alphafold structures for *D. melanogaster* l(2)efl/CryAB (UniProt: A0A0B4KEY5) and *H. sapiens* Alpha-crystallin B chain/CryAB (UniProt: P02511) were superimposed in PyMol.

Cell culture

Cell maintenance

Mouse myogenic C2C12 cells (ATCC, Manassas, VA) were used up to passage number 12. Myoblasts were grown on plastic cell culture dishes in Dulbecco's modified Eagle's medium (DMEM) supplemented with 10% fetal bovine serum and 1% penicillin-streptomycin in a humidified incubator at 37°C and 5% CO_2. When the cells reached 70% confluency, they were detached and plated on a fresh plastic cell culture dish at 1.5×10^5 cells/mL in a 35 mm dish. Once cells were confluent, they were serum limited with differentiation media (DMEM, 2% horse serum, 1% penicillin-streptomycin) and allowed to differentiate. The media for growth or differentiation was replaced daily.

In vitro phosphorylation assay

C2C12 cells were seeded in a 60 mm cell dish at 1.5×10^5 cells/mL. The cells were differentiated to day 3 and treated for 24 hours with WZ4003 at a final concentration of either 4 μM or 6 μM in fresh differentiation media. After 24 hours, the cells were collected into in vitro phosphorylation lysis buffer [400 mM Tris–HCl (pH 7.5), 10 mM $MgCl_2$, 200 μM $CaCl_2$, 1 mM DTT, 1% Triton-100] and homogenized with a tissue homogenizer. The resulting cell lysates were incubated in an ice bath for 20 minutes and centrifuged for 15 minutes at 4°C before removing the supernatant to a new tube. A Bicinchoninic acid (BCA) assay was used to determine the total protein concentration and equal amounts of each cell lysate were split into 2 groups: without ATP or to a final concentration of 5 mM. After incubation for 30 minutes at 30°C, SDS sample buffer was added before Western blotting. Membranes were probed with anti-NUAK1/ARK5 22723-1-AP (ThermoFisher Scientific, Waltham, MA), anti-CryAB ab13497 (Abcam, Waltham, MA), or anti-pCryAB ADI-SPA-227 (Enzo, Farmingdale, NY). Secondary antibody and total protein stain are described above.

Quantitation and statistical analysis

Pupal case muscle contraction

Pupae of the indicated genotype were adhered to a glass slide with a drop of nail polish. All pupae were oriented with dorsal side up and imaged on a Leica M165FC stereoscope. Image J was used to measure the length (l) and width (w) of each pupae and the axial ratio (l/w) was calculated in Excel. All data was imported into Prism to generate a box and whiskers plot. $N \geq 20$ for each genotype.

Muscle abnormalities

Embryos from parents of the genotype *Mef2* > *NUAK RNAi*, *Mef2* > *NUAK K99R*, *Mef2* > *NUAK E197K*, or *Mef2* > *NUAK T226A* were collected at 25°C and transferred to 31°C at the L1 stage. Wandering L3 larvae were dissected in PBS. The resulting muscle carcasses were fixed in 4% methanol-free formaldehyde (Polysciences, Warrington, PA) for 15 minutes at room temperature and washed three times in PBST (phosphate buffered saline + 0.5% Tween) before incubating with phalloidin 488 (1:400) and Hoechst (1:400). For each muscle carcass, 7 distinct muscle fibers ([VL1, VL2, VL3, VL4, LO1, LL1, and segment border muscle (SBM)] from 8 randomly selected abdominal hemisegments were examined under the Zeiss 700 confocal microscope. The number of normal or defective muscles for each larvae was divided by the total number of muscles to calculate the percentage of muscle defects. $N \geq 17$ for each genotype.

Results

NUAK kinase activity is required throughout muscle development and growth

We previously characterized an ethyl methanesulfonate (EMS)-induced stop codon allele in the *Drosophila NUAK* ($NUAK^{R829*}$) gene for its role in autophagic protein degradation (Brooks *et al.* 2020). Since this mutation results in a stop codon that lies outside of the evolutionarily conserved kinase domain (Fig. 1a), we sought to evaluate the contribution of NUAK kinase activity. CRISPR/Cas9 techniques were utilized to create a kinase-dead form of NUAK by mutating a conserved lysine residue required for catalytic activity ($NUAK^{K99R}$) (Carrera *et al.* 1993; Meharena *et al.* 2016). Sanger sequencing of PCR-amplified genomic DNA from heterozygous $NUAK^{K99R}$/+ individuals confirmed the presence of the desired nucleotide alteration (AAA→CGC) that resulted in a lysine to arginine (K→R) mutation in the active site (Fig. 1b). This new allele provides an entryway to examine the direct contribution of NUAK kinase activity during *Drosophila* development.

Lethal phase analysis was performed to compare the relative allelic strength of the $NUAK^{R829*}$ or $NUAK^{K99R}$ mutations (Fig. 1c). Both *WT* (w^{1118}/w^{1118} or w^{1118}/*Canton-S*) and heterozygous *NUAK* ($NUAK^{R829*}$/+ and $NUAK^{K99R}$/+) controls largely enclosed as adults, with some lethality occurring at the embryonic to L1 transition. The majority of homozygous $NUAK^{R829*}/NUAK^{R829*}$ individuals were lethal at the pupal stage, consistent with our previous characterization (Brooks *et al.* 2020). In contrast, approximately 60% of homozygous $NUAK^{K99R}/NUAK^{K99R}$ embryos failed to hatch into L1 larvae and did not survive to pupation. To assess if this embryonic lethality in our kinase-dead embryos may be due to abnormal myogenesis, we analyzed the musculature of stage 16 embryos. The stereotypical muscle pattern present in *WT* embryos (Fig. 1d, left panel) was largely preserved in $NUAK^{K99R}/NUAK^{K99R}$ embryos (Fig. 1e, left panel), while occasionally we observed muscles that were narrower in width in mutant embryos (asterisks, inset). With no obvious defects in myoblast fusion or muscle

patterning, we next assessed sarcomere formation. Analysis of *WT* L1 larvae soon after hatching revealed a regular spacing of sarcomeres marked by sls-GFP (Fig. 1d, right panel). $NUAK^{K99R}$/$NUAK^{K99R}$ L1 larvae also showed relatively normal sarcomeres, but a higher prevalence of thinner muscles than observed in mutant embryos of the same genotype (Fig. 1e, asterisks, inset). Embryonic muscles marked by sls-GFP from either control (Supplementary Video 1) or $NUAK^{K99R}$/$NUAK^{K99R}$ homozygotes (Supplementary Video 2) showed no obvious difference in contractile ability in live imaging experiments. These data together argue that during embryogenesis, muscle development largely proceeds as normal, with minor contributions of NUAK to the final width of individual muscles.

Since most homozygous $NUAK^{K99R}$/$NUAK^{K99R}$ larvae do not survive until the L3 stage for the analysis of muscle morphology, we leveraged the spatial and temporal control of the Gal4/UAS system to assess the impact of mutations that alter kinase activity. Three independent amino acid changes were generated within the kinase domain: (1) K99R within subdomain II; (2) E197K within subdomain VIb; and (3) T226A in the T-loop region of the kinase domain (Fig. 2a). The glutamic acid at position 197 was mutated to mimic a missense mutation that disrupted muscle architecture in *C. elegans unc-82* mutants (Hoppe *et al.* 2010). Finally, the conserved threonine located within the T-loop of NUAK was altered to an alanine (T226A) to abolish phosphorylation by upstream kinases (Yeh *et al.* 2010; Sun *et al.* 2013).

We first tested whether overexpression of each mutation on its own caused dominant effects by monitoring pupal length as a proxy for muscle contraction (LaBeau-DiMenna *et al.* 2012; Brooks *et al.* 2020). During the larval to pupal transition, shortening of the body wall muscles ensures a stereotypical pupal case axial ratio (length/width) of ~3 for *WT* (Fig. 2b). Under control of the *Mef2* promoter, expression of 2 irrelevant UAS lines (*Mef2* > *GFP RNAi* or *Mef2* > *lacZ*) exhibited normal muscle contraction. In contrast, *Mef2* > *NUAK RNAi* individuals showed an increased axial ratio in the range of 4.6–5.9 and thus served as a positive control (Brooks *et al.* 2020). Myofiber expression of transgenes that abolish key residues required for NUAK catalytic activity (*Mef2* > *NUAK K99R*, *Mef2* > *NUAK E197K*) or activation of kinase activity (*Mef2* > *NUAK T226A*) each showed a range of pupal case lengths that were increased compared to controls, indicating defective muscle contraction.

To examine if these mutant transgenes also cause morphological defects similar to those we previously described for *NUAK RNAi* (Brooks *et al.* 2020), we examined F-actin in L3 muscles. Indeed, expression of *NUAK K99R*, *NUAK E197K*, or *NUAK T226A* using *Mef2*-Gal4 in a *WT* background caused a range of sarcomere abnormalities, including thinning muscles and/or a loss of sarcomere patterning (Fig. 2c). The average percentage of muscles that exhibited morphological abnormalities in *Mef2* > *NUAK K99R* or *Mef2* > *NUAK E197K* L3 larvae was greater than 80%, with a penetrance similar to *Mef2* > *NUAK RNAi* (Fig. 2d). Expression of the *NUAK T226A* transgene exhibited milder defects, whereby approximately 40% of muscles showed aberrant muscle morphology. Similar results were obtained for dominant overexpression of kinase mutations using the muscle driver *C57*-Gal4 (Supplementary Fig. 1a–d).

Since *Mef2* turns on transgene expression at embryonic stage 12 and remains elevated in muscle tissue throughout larval development (Ranganayakulu *et al.* 1996), we next utilized the post-embryonic muscle *G7*-Gal4 driver to assess if NUAK kinase activity is required in contractile larval muscles. Few abnormalities were observed in *G7* > *NUAK RNAi* muscles, likely due to the relatively late temporal expression of the *G7* driver in knocking down *NUAK mRNA* compared to *Mef2* (Fig. 2c, d). Both *G7* > *NUAK K99R* or *G7* > *NUAK E197K* showed extensive muscle phenotypes, while those observed with expression of the *NUAK T226A* were weaker. Postembryonic expression of the *G7* promoter was confirmed with a UAS-based *mCherry::NLS* (*mCh::NLS*) construct. *Mef2* > *mCh::NLS* was apparent in all muscles by the end of myogenesis in stage 16 embryos, while *G7* > *mCh::NLS* was undetectable (Fig. 2e). These data together confirm that key residues in the kinase domain of NUAK are essential to maintain normal muscle structure during larval muscle growth and/or contraction.

NUAK promotes CryAB phosphorylation

We previously conducted a Y2H screen with full-length NUAK and identified physical interactions between NUAK-Filamin and NUAK-Stv (Brooks *et al.* 2020). Two additional proteins that emerged as high-confidence interacting proteins were Paramyosin (Prm) and l(2)efl/CryAB. In *C. elegans*, Prm genetically interacts with the NUAK ortholog Unc-82 (Schiller *et al.* 2017). Clones containing the smallest region of either Prm (AA589-671) or CryAB (AA79-154) that physically associated with NUAK were verified in a 1 by 1 interaction assays. The previously published SMAD-SMURF interaction was used as a positive control (Colland *et al.* 2004). Empty bait vector with Prm or CryAB yielded no yeast growth, while an interaction between NUAK-Prm or NUAK-CryAB could be reproduced in 3 independent biological replicates (Fig. 3a).

We next tested if a disruption in NUAK function altered the distribution of CryAB or Prm in muscle tissue. CryAB is detected at the Z-disc and largely excluded from other regions that are enriched for F-actin in *Mef2* > *lacZ* control muscles (Fig. 3b) (Wójtowicz *et al.* 2015). In both *Mef2* > *NUAK RNAi* (Brooks *et al.* 2020) or *Mef2* > *NUAK* kinase mutants, larger areas that lack F-actin instead accumulate CryAB in an abnormal pattern. The specificity of the CryAB antibody was confirmed with immunostaining and Western blotting of *CryAB RNAi* muscles (Supplementary Fig. 2). In contrast, immunostaining for Prm did not reveal similar results. In *NUAK RNAi* or upon expression of NUAK kinase domain mutations, areas of muscle tissue without F-actin also lacked Prm (Supplementary Fig. 3). Thus, while NUAK physically interacts with both proteins, the subcellular fate of CryAB or Prm is different when NUAK function is compromised.

The necessity of NUAK kinase activity obviates the question of whether CryAB could be a target substrate. To examine if phosphorylation could be detected, we first overexpressed NUAK in muscle tissue and assessed the migration pattern of CryAB by Western blotting. Slower migrating bands suggestive of a post-translational modification (PTM) were apparent for CryAB upon overexpression of full-length NUAK (NUAK FL) (Fig. 4a). These putative phospho-CryAB bands were either reduced in intensity or not present after induction of *NUAK RNAi* or upon dominant expression of kinase-dead (*NUAK K99R*) or inactivated (*NUAK T226A*) NUAK. Next, we treated lysates derived from muscles overexpressing NUAK with λ-phosphatase and observed the disappearance of higher migrating bands corresponding to phosphorylated CryAB species (Fig. 4b), thus proving that NUAK influences CryAB phosphorylation.

Since the T226A mutation in NUAK abolished phosphorylation of CryAB, we tested if changing this threonine to a glutamic acid (T226E) could functionally mimic NUAK activation. First, we tested the specificity of the threonine mutation using a

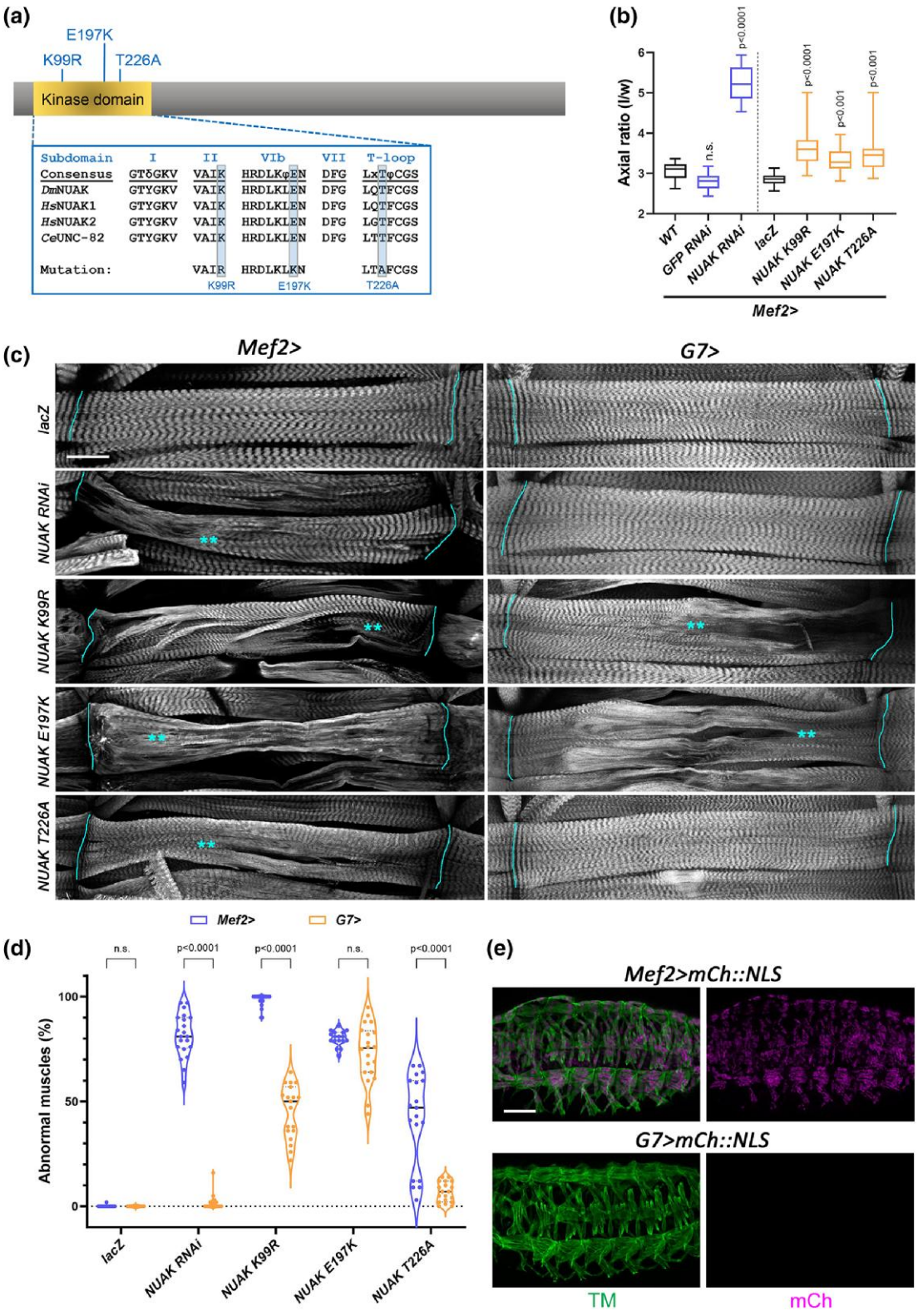

Fig. 2. Kinase activity is essential to maintain the architecture of contractile muscles. a) Schematic of the NUAK protein showing the location of UAS-based kinase domain mutations. b) Box and whisker plot quantifying the relative amount of muscle contraction at the L3 to pupal transition. Control pupae (*WT*, *Mef2* > *GFP RNAi*, or *Mef2* > *lacZ*) exhibit a standard axial (length to width) ratio consistent with normal muscle contraction. RNAi knockdown of NUAK or expression of individual kinase domain mutations (K99R, E197K, or T226A) in a *WT* background under control of the *Mef2* promoter significantly impairs muscle contraction, resulting in increased axial ratios. $N \geq 20$ for each genotype. c) Representative maximum intensity projections of L3 larval muscles stained with phalloidin to visualize F-actin. UAS-based constructs expressing either *NUAK RNAi* or NUAK kinase domain mutations with *Mef2*-Gal4 or *G7*-Gal4. Lines indicate muscle attachment sites and asterisks are located next to regions that show abnormal F-actin morphology. Scale bar, 25 µm. d) Violin plot with individual data points showing the percentage of muscles in panel C exhibiting abnormal muscle morphology. e) Maximum intensity projections of *Mef2* > *mCh::NLS* (top panels) or *G7* > *mCh::NLS* (bottom panels) embryos stained with anti-Tropomyosin (TM) confirm that the *G7* promoter is not expressed during embryogenesis. Scale bar, 50 µm.

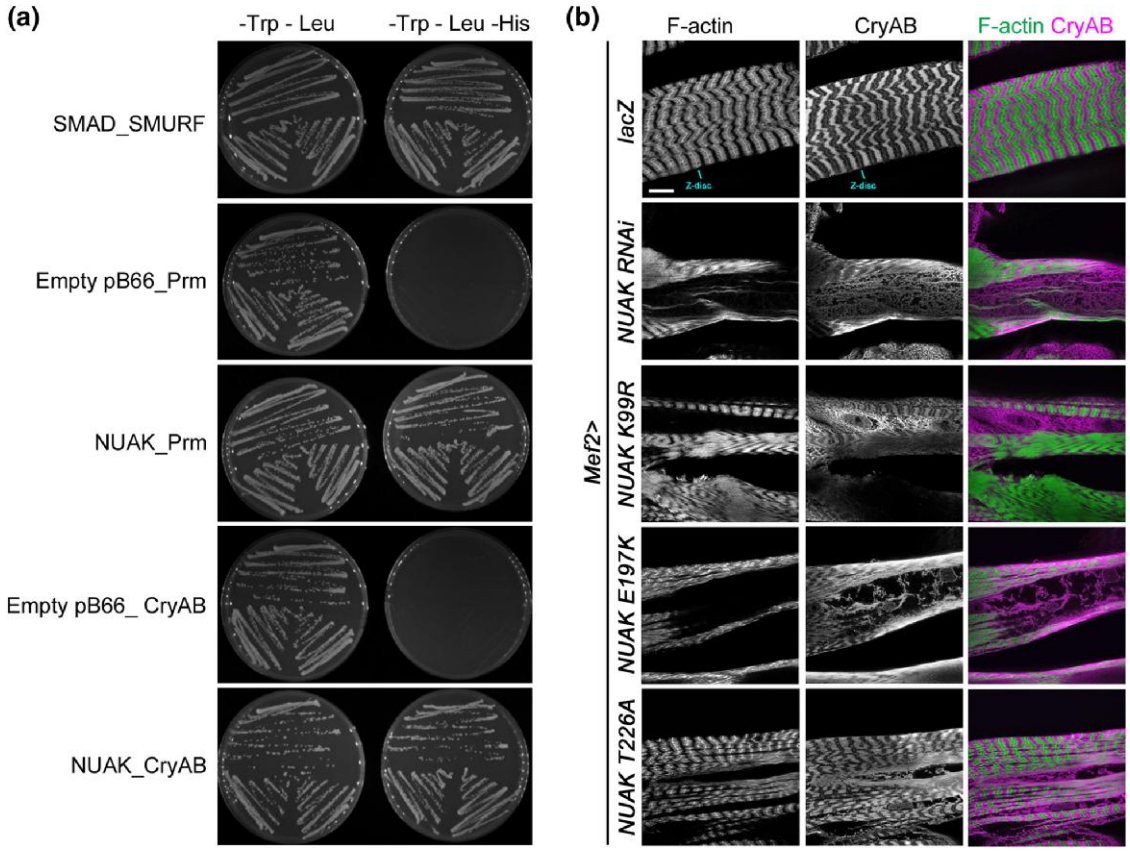

Fig. 3. CryAB physically interacts with NUAK and accumulates abnormally in *NUAK* mutant muscles. a) Y2H experiments test for an interaction between bait and prey proteins. Yeast growth on media lacking Trp and Leu verify the presence of the bait and prey plasmids. Colony growth on selective media plates (–Trp –Leu –His) indicates a physical interaction between SMAD_SMURF (positive control), NUAK_Prm, and NUAK_CryAB. No growth was observed for the empty bait vector with Prm or CryAB. Three independently transformed yeast clones were tested for each bait-prey pair. b) L3 larval muscles stained with phalloidin to visualize F-actin or an antibody raised against CryAB. F-actin and CryAB overlap at the Z-disc and can be observed in complementary patterns in control *Mef2* > *lacZ* muscles. Muscle expression of *NUAK RNAi* or *NUAK* kinase domain mutations (*K99R*, *E197K*, or *T226A*) all show abnormal accumulation of CryAB in regions that lack F-actin. Scale bar, 50 µm.

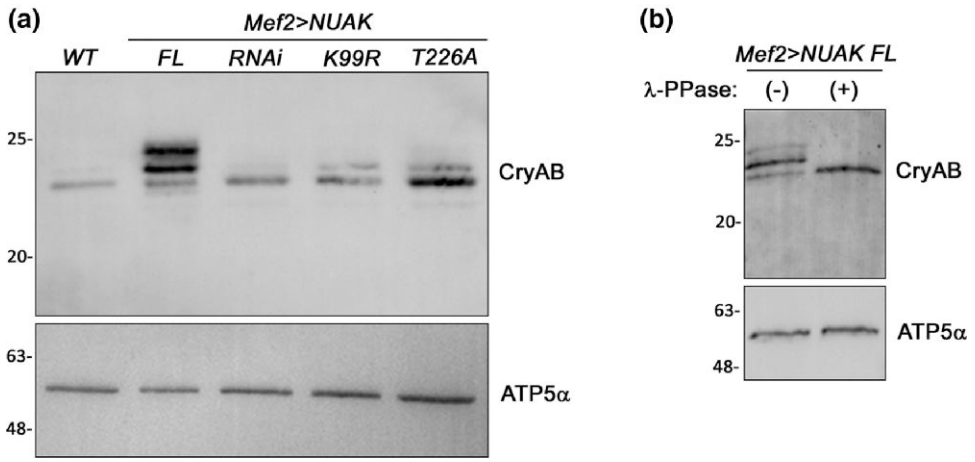

Fig. 4. NUAK promotes CryAB phosphorylation. a) Western blot showing the migration pattern of CryAB bands in the indicated genotypes. Overexpression of *NUAK FL* results in higher migrating forms of CryAB. Knockdown of NUAK protein using RNAi or dominant expression of *NUAK K99R* or *NUAK T226A* reduces the amount of slower migrating CryAB bands. b) The multiple bands observed upon *Mef2* > *NUAK FL* expression collapse into a single band upon λ-PPase treatment. ATP5α is used as a loading control.

phospho-specific antibody (pNUAK) generated against the corresponding threonine (T211) residue in a synthetic human ARK5 peptide. Seven of the eight amino acids, in addition to T211/T226, are conserved between HsARK5, HsSNARK, DsNUAK (Fig. 5a). This pNUAK antibody did not detect endogenous protein in control *lacZ* muscle lysates, but effectively recognized elevated levels of K99R, E197K (Fig. 5b), or NUAK FL (Supplementary Fig. 4) driven by *Mef2*-Gal4. As expected, the T226A or T226E mutations

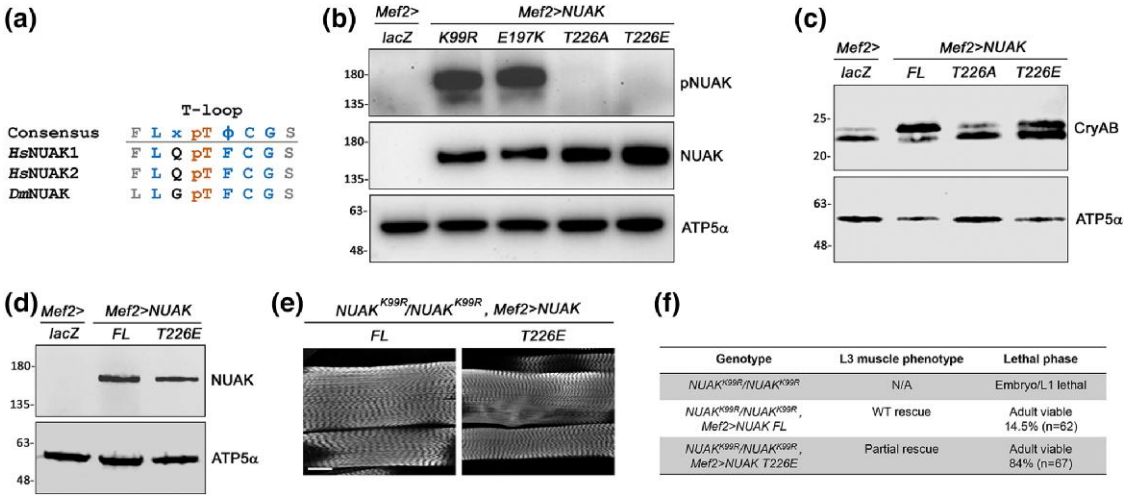

Fig. 5. Phospho-mimetic *NUAK T226E* rescues $NUAK^{K99R}/NUAK^{K99R}$ mutant phenotypes. a) Location of the pT residue in the conserved T-loop region of HsNUAK1/ARK5, HsNUAK2/SNARK, and DsNUAK. b) Confirmation of the *T226A* or *T226E* mutation by Western blotting. The pNUAK Ab, raised against HsNUAK1, recognizes overexpressed *NUAK K99R* and *NUAK E197K*, but not mutation of the *T226* residue. c) Phospho-mimetic *T226E* is sufficient for CryAB phosphorylation and *T226A* reduced this modification. *NUAK FL* was used as a positive control. (d-f) Rescue of $NUAK^{K99R}/NUAK^{K99R}$ mutants at 25°C with muscle expression of *NUAK FL* or *NUAK T226E*. d) Western blotting confirms the expression of *NUAK FL* or *NUAK T226E*. ATP5α is used as a loading control. e) L3 larval muscles stained for F-actin have largely WT sarcomeres. Scale bar, 50 μm. f) Table summarizes lethality and muscle phenotype.

failed to be recognized by the pT211 Ab (Fig. 5b), but expression of each produced different outcomes. Consistent with Fig. 4a, T226A lysates reduced CryAB phosphorylation, while expression of T226E mimicked phosphorylation events on CryAB similar to that of FL overexpression (Fig. 5c).

We next tested whether T226E is sufficient to rescue $NUAK^{K99R}/NUAK^{K99R}$ mutants. NUAK FL was used as a positive control since we previously demonstrated that muscle expression of this transgene rescued the generative muscle phenotype in $NUAK^{R829^*}/NUAK^{R829^*}$ mutants (Brooks *et al.* 2020). First, we confirmed protein expression of the NUAK FL or T226E transgenes in larval lysates (Fig. 5d) and then assessed the extent of rescue in L3 muscles. Indeed, *Mef2*-induced expression of NUAK FL or T226E in homozygous $NUAK^{K99R}/NUAK^{K99R}$ muscles was largely normal (Fig. 5e). Moreover, this muscle expression produced viable adults (Fig. 5f), showing that T226E can functionally rescue aspects of NUAK biology throughout all of muscle development.

Next, we took advantage of an HA-tagged version of CryAB to map phosphorylation sites. First, we needed to confirm that the 3xHA affinity tag did not interfere with the in vivo NUAK-CryAB complex. Therefore, we performed PLA experiments using a rabbit antibody against NUAK and a mouse antibody that detects the HA tag on the C-terminus of CryAB. *LacZ* control muscles showed an average of ~2 puncta/50 μm^2 (Fig. 6a). The number of PLA(+) structures representing the NUAK-CryAB complex was increased upon muscle expression of CryAB::3xHA alone and in the presence of NUAK FL overexpression (Fig. 6b). Controls for the PLA(+) or (–) probes only did not produce any signal.

While expression of CryAB::3xHA alone in muscle induced more phosphorylation than controls, this PTM was further enhanced upon co-expression with NUAK (Fig. 6c). Hence, this hyper-phosphorylated CryAB was isolated from muscle tissue using anti-HA beads and run on an SDS-PAGE gel followed by Coomassie staining. Bands corresponding to CryAB were removed, trypsin digested, and subjected to MS analysis (Fig. 6d). Total CryAB sequence coverage was ~88% after three independent biological replicates. Attempts to improve peptide coverage corresponding to the extreme N- and C-termini with chymotrypsin were not successful. Nevertheless, the trypsin digest experiments revealed 2 putative phosphorylation sites on serine residues located at amino acids 68 and 70 within the same peptide (Fig. 6e, f).

Each monomer of CryAB has 3 distinct regions: a conserved α-crystallin domain (ACD) that is comprised of 8 antiparallel beta strands flanked by an unstructured N-terminal region (NTR) and a shorter C-terminal region (CTR) (Bakthisaran *et al.* 2016; Dimauro and Caporossi 2022). The general location of these 2 phosphoresidues is conserved in human CryAB, with *Drosophila* S68 or S70 corresponding to human T63 or S66, respectively (Fig. 7a). The location of these phospho-S/T residues were mapped onto the *Drosophila* or human CryAB Alphafold protein structures. S68 lies in a small loop region that precedes the first β-sheet of the ACD and S70 is the first AA of this β-sheet (Fig. 7b). To assess if serine 68 and/or serine 70 are indeed phosphorylated by NUAK, we mutated each of these residues to either alanine (to prevent phosphorylation) or glutamic acid (phospho-mimic). Overall protein levels of CryAB were increased upon expression of WT or phospho-mutant versions of CryAB compared to lacZ control lysates (Fig. 7c). Slower migrating, or phosphorylated forms of CryAB, were reduced upon expression of S68A or S70A and completely abolished in the S68A/S70A double mutant. Phosphorylated versions of CryAB were present upon expression of S68E or S70E, with the latter showing multiple bands. Together, these data demonstrate that S68 and S70 are both targeted for phosphorylation and the S70E phospho-mimetic induces hyperphosphorylation.

To test if human NUAK1 or human NUAK2 function similar to its *D. melanogaster* counterpart, we generated transgenic flies expressing either full-length (hNUAK1 or hNUAK2) or kinase-dead (hNUAK1 K84R or hNUAK2 K81R) versions of each protein and expressed them in larval muscle tissue. Expression of only hNUAK1 K84R showed phenotypes similar to expression of *D. melanogaster NUAK RNAi* or the dominant NUAK transgenes (K99R, E197K, T226A), whereby the prevalent phenotype was muscle degeneration and CryAB accumulation (Fig. 7d). These data suggest that there may be shared features between human NUAK1 and fly

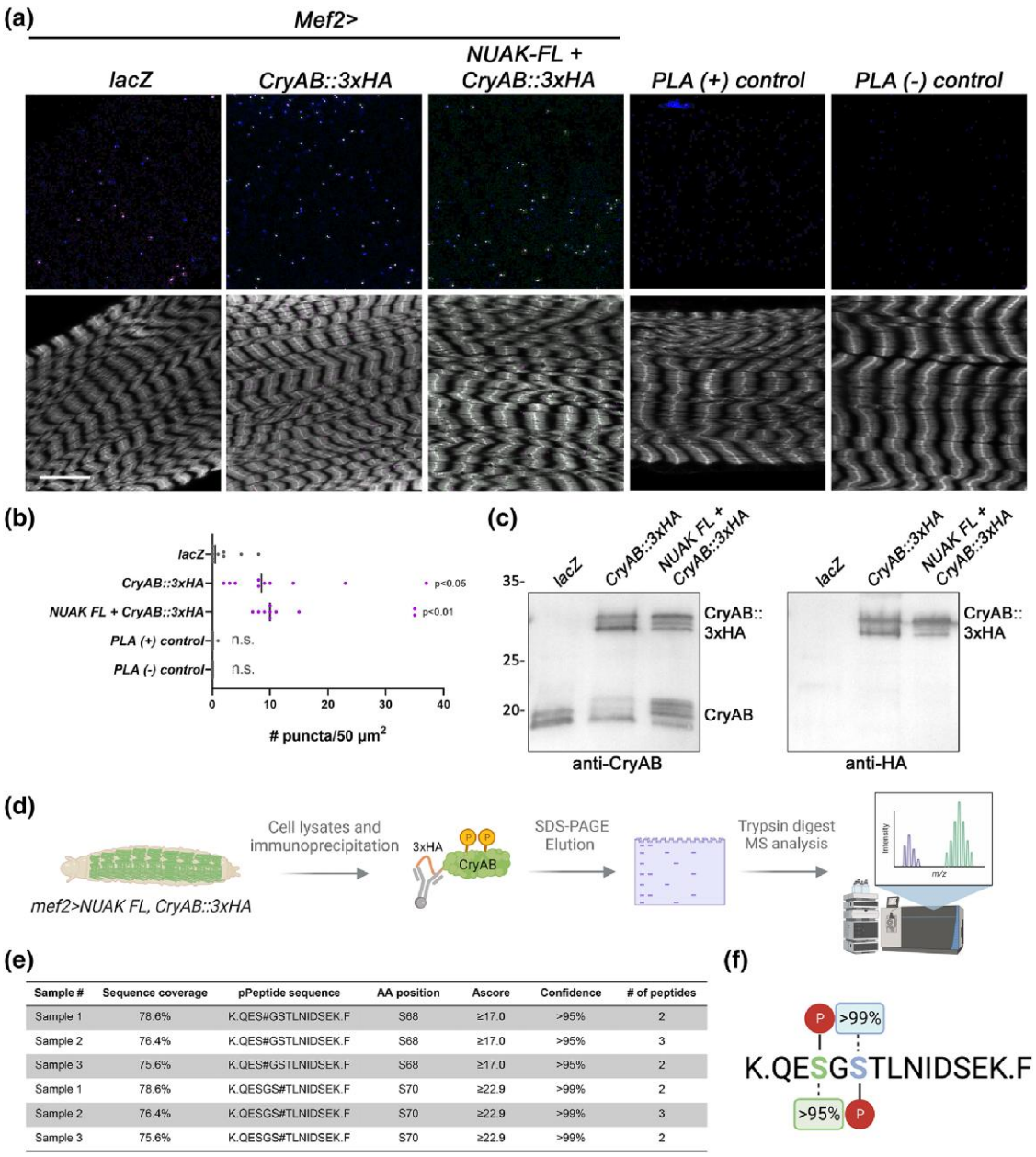

Sample #	Sequence coverage	pPeptide sequence	AA position	Ascore	Confidence	# of peptides
Sample 1	78.6%	K.QES#GSTLNIDSEK.F	S68	≥17.0	>95%	2
Sample 2	76.4%	K.QES#GSTLNIDSEK.F	S68	≥17.0	>95%	3
Sample 3	75.6%	K.QES#GSTLNIDSEK.F	S68	≥17.0	>95%	2
Sample 1	78.6%	K.QESGS#TLNIDSEK.F	S70	≥22.9	>99%	2
Sample 2	76.4%	K.QESGS#TLNIDSEK.F	S70	≥22.9	>99%	3
Sample 3	75.6%	K.QESGS#TLNIDSEK.F	S70	≥22.9	>99%	2

Fig. 6. Determination of phosphorylation sites on CryAB isolated from muscle. a and b) Either endogenous or overexpressed NUAK can form a complex with CryAB as assayed by PLA experiments. a) Maximum intensity projections of L3 muscle tissue (F-actin, lower panels) to visualize the NUAK-CryAB complex (top panels). Scale bar, 25 µm. b) Scatter plot showing an increase in the number of PLA(+) puncta/50 µm^2 for tagged CryAB with and without NUAK compared to *Mef2* > *lacZ* or PLA controls. One-way ANOVA was performed and the indicated *P*-values are in comparison to *lacZ*. $N = 10$. c) Western blots confirm that the 3xHA-tagged version of CryAB is phosphorylated in muscle tissue. Bands corresponding to phosphorylated CryAB can be visualized with either anti-CryAB (left panel) or anti-HA (right panel) upon expression of *Mef2* > *CryAB::3xHA* alone or with *NUAK FL* expression. d) Strategy depicting expression and isolation of CryAB for phosphorylation site identification by MS. e) Table with a summary of phospho-MS experiments. Three independent biological replicates were analyzed with total peptide coverage of CryAB ranging from 75.6–78.6%. Serines corresponding to amino acid residues 68 and 70 were both found to be phosphorylated with confidence values >95%. f) Summary of CryAB phosphosites.

NUAK that affect cellular processes and possibly even common substrates, at least in muscle tissue.

Discussion

In this manuscript, we show that the catalytic activity of NUAK is essential for viability and to prevent muscle degeneration. We verify a physical interaction between NUAK and CryAB and further demonstrate that NUAK promotes the phosphorylation of CryAB at S68 and S70. Since mutations in human Filamin C (FLNC), BAG family molecular chaperone regulator 3 (BAG3), or CRYAB are causative for protein aggregate diseases (Béhin *et al.* 2015; Batonnet-Pichon *et al.* 2017; Fichna *et al.* 2018; Guglielmi *et al.* 2018), our molecular analysis confirms the functional importance of phosphorylation in the prevention of abnormal protein accumulation in muscle tissue.

How do NUAK kinase-dead mutations inhibit phosphorylation? Since the dominant expression of these kinase variants produces phenotypes in the presence of endogenous protein, NUAK may limit phosphotransfer activity via three mechanisms. First, since

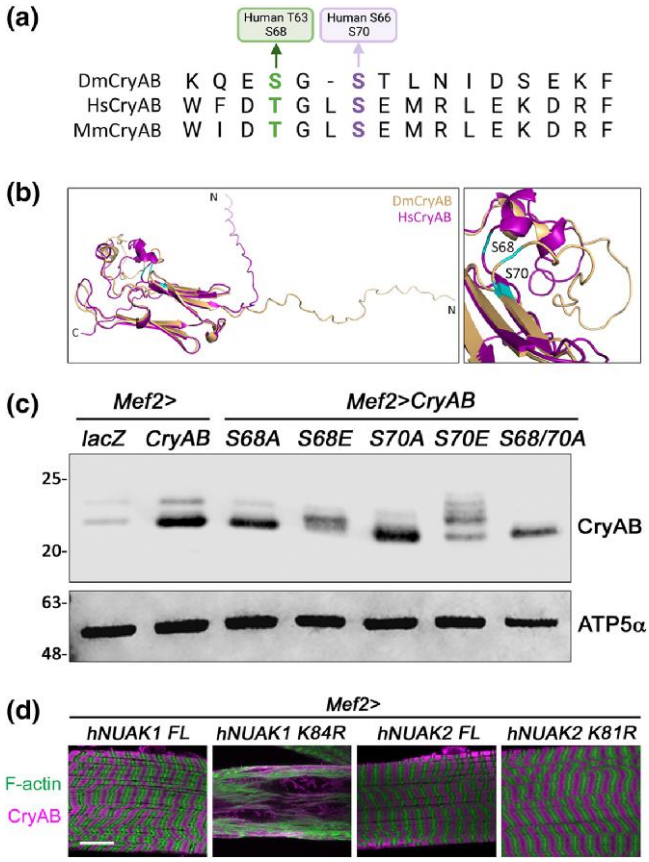

Fig. 7. Functional confirmation of CryAB phosphosites. a) Alignment of CryAB sequences from *D. melanogaster* (Dm), human (Hs), or mouse (Mm) showing conservation of the S and T residues that are modified in *D. melanogaster* CryAB. b) An overlay of the ribbon diagrams for DmCryAB and HsCryAB. The location of S68 and S70 are shown. c) Western blot for CryAB protein upon mutation of S68 and/or S70. No phosphorylation is observed in the S68/S70A double mutation. ATP5α is used as a loading control. d) L3 muscles stained for F-actin or anti-CryAB. Overexpression of kinase-dead hNUAK1 (*Mef2* > *hNUAK1 K84R*), but not hNUAK2 (*Mef2* > *hNUAK2 K81R*), disrupts muscle morphology and causes CryAB accumulation. Scale bar, 25 μm.

the NUAK UAS-expression constructs drive higher levels than seen for endogenous NUAK, stable interactions between NUAK and CryAB could favor the inactive kinase over the active endogenous one—thereby reducing CryAB phosphorylation. Second, if dimerization of NUAK is required for kinase activity, interactions between endogenous NUAK and its kinase-dead counterpart could titrate out kinase activity of WT NUAK. In addition, or alternatively, substrate proteins may initially interact with the catalytic pocket of kinase-dead NUAK but remain in the active site for longer than usual if the protein cannot be released. This would effectively limit the amount of substrate available for cellular functions.

Multiple studies have shown that a loss of AMPK-related kinase activation in the T-loop reduces catalytic activity (Bright *et al.* 2009; Yeh *et al.* 2010; Sun *et al.* 2013; Herzig and Shaw 2018). While we also observed a reduction in NUAK function upon expression of T226A, the percentage of muscle abnormalities was less severe compared to K99R or E197K. Maybe the phosphate appended to T226 is somewhat stable on the pool of endogenous NUAK and can outcompete the ectopic NUAK T226A protein for substrate phosphorylation. It is also possible that additional amino acids aside from T226 are regulated by phosphorylation. In addition to the T-loop residue in human NUAK1, amino acid 600 is also phosphorylated by Akt (Suzuki *et al.* 2003). *D. melanogaster* lacks this conserved Akt phosphosite but may have others yet to be determined. An additional unknown is the identity of the upstream kinase(s) that phosphorylate(s) NUAK in response to muscle contraction and/or increased mechanical tension.

Multiple pieces of evidence provide support for NUAK-mediated phosphorylation of CryAB. First, a physical interaction between NUAK and CryAB was identified by Y2H. Overexpression of WT or activated NUAK (T226E) increased the pool of phosphorylated CryAB, while kinase-dead (K99R, E197K) or inactivated (T226A) NUAK reduced this modification. Due to the inability to purify full-length *D. melanogaster* NUAK, we have been unable to show that CryAB phosphorylation is directly mediated by NUAK. It is possible that NUAK phosphorylates an intermediate kinase that in turn acts on CryAB. Purified p44/42 mitogen-activated protein kinase (MAPK) and mitogen-activated protein kinase-activated protein-2 (MAPKAP kinase-2) can phosphorylate S45 and S59 in human CryAB (Kato *et al.* 1998). Phosphorylation of CryAB S59 is also increased during C2C12 differentiation, in C2C12 cells subjected to electrical pulse stimulation (EPS), and in resistance exercise-loading in human skeletal muscle (Singh *et al.* 2010; Reimann *et al.* 2017; Jacko *et al.* 2020). Inhibition of NUAK1/ARK5 kinase activity using the NUAK1-specific inhibitor WZ4003 in C2C12 cells shows a reduction in phospho-S59 levels (Supplementary Fig. 5). While more experiments need to be done to confirm a direct relationship between the phosphorylation of CryAB by mammalian NUAK1, these data suggest possible conservation of the NUAK-CryAB signaling axis.

Even though hCryAB is ubiquitously expressed, dominant or recessive mutations identified in multiple patients can result in multisystem disorders characterized by cardiomyopathies, cataracts, or skeletal myopathies (Dimauro *et al.* 2018; Dimauro and Caporossi 2022). The correlation between individual molecular mutations, disease onset, and variable expressivity is not well understood at the tissue or organismal level. Chaperone functions for CryAB are largely thought to prevent the abnormal accumulation of cellular proteins. While specific binding partners of CryAB, such as Desmin, have been verified (Wang *et al.* 2003; Jacko *et al.* 2020), the promiscuous nature of CryAB in other contexts has made it difficult to pinpoint its molecular function. In our hands, incubation of larval lysates with *CryAB::3xHA* in pull-down experiments produced hundreds of proteins in experimental vs control experiments. This suggests that interactions of CryAB with other proteins may be tightly regulated in intact cells, but this contextual specificity is lost outside of the normal cellular environment.

Numerous studies demonstrate that the oligomerization state of mammalian CryAB/HSPB5 is crucial for the regulation of chaperone activity (Bakthisaran *et al.* 2016; Dimauro *et al.* 2018; Dimauro and Caporossi 2022). Monomeric CryAB assembles into dimers via interactions between antiparallel beta strands located within the ACD (Bagnéris *et al.* 2009; Jehle *et al.* 2010; Baranova *et al.* 2011). Intermolecular contacts in the CTR of three CryAB dimers form a hexameric unit which can form higher order multimers (12-mer or 24-mer) largely mediated by the NTR (Peschek *et al.* 2009; Braun *et al.* 2011; Jehle *et al.* 2011). It is proposed that the equilibrium between smaller and larger oligomeric CryAB complexes determines client substrate interactions. Multimeric species may act as storage forms of CryAB, whereas smaller oligomers exhibit chaperone activity since potential substrate binding sites within the NTR, ACD, or CTR are exposed for protein interactions.

Phosphorylation alters the distribution of CryAB toward lower oligomeric species (Ito *et al.* 2001; Bakthisaran *et al.* 2016). In particular, mimicking phosphorylation events on three known serine residues in mammalian CryAB (S19D/S45D/S59D) reduces the mean diameter of CryAB complexes and decreases stability as assessed by urea denaturation experiments (Ahmad *et al.* 2008). Generally, ageing, stress, or disease increases the relative pool of phosphorylated CryAB. Both aged muscle tissue and eye lenses with cataracts have increased levels of phosphorylated CryAB that partition into the insoluble fraction (Kato *et al.* 2002; Ueda *et al.* 2002; Yamaguchi *et al.* 2007; Huang *et al.* 2011). Heat stress or oxidative stress produces a similar phenomenon in various cell types including neurons (Bakthisaran *et al.* 2016). As of yet, there is no clear consensus on the biological implications of CryAB phosphorylation, which have been shown to be beneficial or deleterious, depending on the cellular context. In terms of autophagy, we hypothesize that NUAK may activate CryAB to unfold aggregates to prevent abnormal protein accumulation. Future experiments will focus on clarifying the molecular role of CryAB phosphorylation in muscle tissue.

Data availability

The authors confirm that the data supporting the findings of this study are available within the article and its Supplementary materials.

Supplemental material available at GENETICS online.

Acknowledgments

Thanks to colleagues Lori Wallrath (C57-Gal4), Mary Baylies (G7-Gal4), and Maxim Frolov (sls-GFP) for sharing fly stocks. A special thank you to Aaron Johnson for advice on live imaging experiments. Stocks obtained from the BDSC are supported by a grant from the Office of the Director of the National Institue of Health under Award Number P40OD018537. We also thank FlyORF for supplying the CryAB::3xHA line. Thanks to Ross Tomaino at the Taplin Mass Spectrometry Facility in Harvard Medical School for phosphosite identificaiton.

Funding

This study was supported by the National Institute of Arthritis and Musculoskeletal and Skin Diseases (NIAMS) of the National Institutes of Health (NIH) under award number RO1AR060788 to E.R.G. Thanks to the Kansas State University Johnson Cancer Research Center (JCRC) for travel funds to Z.Z. and Y.G.

Conflicts of interest

The author(s) declare no conflict of interest.

Literature cited

Ahmad MF, Raman B, Ramakrishna T, Rao CM. 2008. Effect of phosphorylation on alpha B-crystallin: differences in stability, subunit exchange and chaperone activity of homo and mixed oligomers of alpha B-crystallin and its phosphorylation-mimicking mutant. J Mol Biol. 375(4):1040–1051. doi:10.1016/j.jmb.2007.11.019.

Alessi DR, Sakamoto K, Bayascas JR. 2006. LKB1-dependent Signaling pathways. Annu Rev Biochem. 75(1):137–163. doi:10.1146/annurev.biochem.75.103004.142702.

Bagnéris C, Bateman OA, Naylor CE, Cronin N, Boelens WC, Keep NH, Slingsby C. 2009. Crystal structures of alpha-crystallin domain dimers of alphaB-crystallin and Hsp20. J Mol Biol. 392(5):1242–1252. doi:10.1016/j.jmb.2009.07.069.

Bakthisaran R, Akula KK, Tangirala R, Rao CM. 2016. Phosphorylation of αB-crystallin: role in stress, aging and patho-physiological conditions. Biochim Biophys Acta. 1860(1):167–182. doi:10.1016/j.bbagen.2015.09.017.

Baranova EV, Weeks SD, Beelen S, Bukach OV, Gusev NB, Strelkov SV. 2011. Three-dimensional structure of α-crystallin domain dimers of human small heat shock proteins HSPB1 and HSPB6. J Mol Biol. 411(1):110–122. doi:10.1016/j.jmb.2011.05.024.

Batonnet-Pichon S, Behin A, Cabet E, Delort F, Vicart P, Lilienbaum A. 2017. Myofibrillar myopathies: new perspectives from animal models to potential therapeutic approaches. J Neuromuscul Dis. 4(1):1–15. doi:10.3233/JND-160203.

Béhin A, Salort-Campana E, Wahbi K, Richard P, Carlier RY, Carlier P, Laforêt P, Stojkovic T, Maisonobe T, Verschueren A, *et al.* 2015. Myofibrillar myopathies: state of the art, present and future challenges. Rev Neurol (Paris). 171(10):715–729. doi:10.1016/j.neurol.2015.06.002.

Bennison SA, Liu X, Toyo-Oka K. 2022. Nuak kinase signaling in development and disease of the central nervous system. Cell Signal. 100:110472. doi:10.1016/j.cellsig.2022.110472.

Bischof J, Björklund M, Furger E, Schertel C, Taipale J, Basler K. 2013. A versatile platform for creating a comprehensive UAS-ORFeome library in Drosophila. Development. 140(11):2434–2442. doi:10.1242/dev.088757.

Bonnard C, Navaratnam N, Ghosh K, Chan PW, Tan TT, Pomp O, Ng AYJ, Tohari S, Changede R, Carling D, *et al.* 2020. A loss-of-function NUAK2 mutation in humans causes anencephaly due to impaired Hippo-YAP signaling. J Exp Med. 217(12):e20191561. doi:10.1084/jem.20191561.

Braun N, Zacharias M, Peschek J, Kastenmüller A, Zou J, Hanzlik M, Haslbeck M, Rappsilber J, Buchner J, Weinkauf S. 2011. Multiple molecular architectures of the eye lens chaperone αB-crystallin elucidated by a triple hybrid approach. Proc Natl Acad Sci U S A. 108(51):20491–20496. doi:10.1073/pnas.1111014108.

Breitkopf SB, Asara JM. 2012. Determining in vivo phosphorylation sites using mass spectrometry. Curr Protoc Mol Biol;98:18.19.1–-18.19.27. doi:10.1101/2022.10.10.511510

Bright NJ, Thornton C, Carling D. 2009. The regulation and function of mammalian AMPK-related kinases. Acta Physiol (Oxf). 196(1):15–26. doi:10.1111/j.1748-1716.2009.01971.x.

Brooks D, Bawa S, Bontrager A, Stetsiv M, Guo Y, Geisbrecht ER. 2022. Independent pathways control muscle tissue size and sarcomere remodeling. Dev Biol. 490:1–12. doi:10.1016/j.ydbio.2022.06.014.

Brooks D, Naeem F, Stetsiv M, Goetting SC, Bawa S, Green N, Clark C, Bashirullah A, Geisbrecht ER. 2020. Drosophila NUAK functions with Starvin/BAG3 in autophagic protein turnover. PLoS Genet. 16(4):e1008700. doi:10.1371/journal.pgen.1008700.

Carrera AC, Alexandrov K, Roberts TM. 1993. The conserved lysine of the catalytic domain of protein kinases is actively involved in the phosphotransfer reaction and not required for anchoring ATP. Proc Natl Acad Sci U S A. 90(2):442–446. doi:10.1073/pnas.90.2.442.

Chen C, Turk BE. 2010. Analysis of serine-threonine kinase specificity using arrayed positional scanning peptide libraries. *Curr Protoc Mol Biol*; 91:18.14.1–18.14.15. doi:10.1002/0471142727.mb1814s91

Colland F, Jacq X, Trouplin V, Mougin C, Groizeleau C, Hamburger A, Meil A, Wojcik J, Legrain P, Gauthier J-M. 2004. Functional proteomics mapping of a human signaling pathway. Genome Res. 14(7):1324–1332. doi:10.1101/gr.2334104.

Dente L, Vetriani C, Zucconi A, Pelicci G, Lanfrancone L, Pelicci PG, Cesareni G. 1997. Modified phage peptide libraries as a tool to study specificity of phosphorylation and recognition of tyrosine containing peptides. J Mol Biol. 269(5):694–703. doi:10.1006/jmbi.1997.1073.

Dimauro I, Antonioni A, Mercatelli N, Caporossi D. 2018. The role of αB-crystallin in skeletal and cardiac muscle tissues. Cell Stress Chaperones. 23(4):491–505. doi:10.1007/s12192-017-0866-x.

Dimauro I, Caporossi D. 2022. Alpha B-crystallin in muscle disease prevention: the role of physical activity. Molecules. 27(3):1147. doi:10.3390/molecules27031147.

Fichna JP, Maruszak A, Żekanowski C. 2018. Myofibrillar myopathy in the genomic context. J Appl Genet. 59(4):431–439. doi:10.1007/s13353-018-0463-4.

Guglielmi V, Tomelleri G, Vattemi G. 2018. Myofibrillar myopathies through the microscope: from diagnosis to molecular pathogenesis. Microscopie. 29(1):7325. doi:10.4081/microscopie.2018.7325

Hardie DG. 2011. AMP-activated protein kinase: an energy sensor that regulates all aspects of cell function. Genes Dev. 25(18):1895–1908. doi:10.1101/gad.17420111.

Hastie CJ, McLauchlan HJ, Cohen P. 2006. Assay of protein kinases using radiolabeled ATP: a protocol. Nat Protoc. 1(2):968–971. doi:10.1038/nprot.2006.149.

Herzig S, Shaw RJ. 2018. AMPK: guardian of metabolism and mitochondrial homeostasis. Nat Rev Mol Cell Biol. 19(2):121–135. doi:10.1038/nrm.2017.95.

Hoppe PE, Chau J, Flanagan KA, Reedy AR, Schriefer LA. 2010. Caenorhabditis elegans unc-82 encodes a serine/threonine kinase important for myosin filament organization in muscle during growth. Genetics. 184(1):79–90. doi:10.1534/genetics.109.110189.

Hou X, Liu JE, Liu W, Liu CY, Liu ZY, Sun Z-Y. 2011. A new role of NUAK1: directly phosphorylating p53 and regulating cell proliferation. Oncogene. 30(26):2933–2942. doi:10.1038/onc.2011.19.

Huang CH, Wang YT, Tsai CF, Chen YJ, Lee JS, Chiou S-H. 2011. Phosphoproteomics characterization of novel phosphorylated sites of lens proteins from normal and cataractous human eye lenses. Mol Vis. 17:186–198.

Hudson AM, Petrella LN, Tanaka AJ, Cooley L. 2008. Mononuclear muscle cells in Drosophila ovaries revealed by GFP protein traps. Dev Biol. 314(2):329–340. doi:10.1016/j.ydbio.2007.11.029.

Inazuka F, Sugiyama N, Tomita M, Abe T, Shioi G, Esumi H. 2012. Muscle-specific knock-out of NUAK family SNF1-like kinase 1 (NUAK1) prevents high fat diet-induced glucose intolerance. J Biol Chem. 287(20):16379–16389. doi:10.1074/jbc.M111.302687.

Ito H, Kamei K, Iwamoto I, Inaguma Y, Nohara D, Kato K. 2001. Phosphorylation-induced change of the oligomerization state of alpha B-crystallin. J Biol Chem. 276(7):5346–5352. doi:10.1074/jbc.M009004200.

Jacko D, Bersiner K, Schulz O, Przyklenk A, Spahiu F, Höhfeld J, Bloch W, Gehlert S. 2020. Coordinated alpha-crystallin B phosphorylation and desmin expression indicate adaptation and deadaptation to resistance exercise-induced loading in human skeletal muscle. Am J Physiol Cell Physiol. 319(2):C300–C312. doi:10.1152/ajpcell.00087.2020.

Jehle S, Rajagopal P, Bardiaux B, Markovic S, Kühne R, Stout JR, Higman VA, Klevit RE, van Rossum B-J, Oschkinat H. 2010. Solid-state NMR and SAXS studies provide a structural basis for the activation of alphaB-crystallin oligomers. Nat Struct Mol Biol. 17(9):1037–1042. doi:10.1038/nsmb.1891.

Jehle S, Vollmar BS, Bardiaux B, Dove KK, Rajagopal P, Gonen T, Oschkinat H, Klevit RE. 2011. N-terminal domain of alphaB-crystallin provides a conformational switch for multimerization and structural heterogeneity. Proc Natl Acad Sci U S A. 108(16):6409–6414. doi:10.1073/pnas.1014656108.

Kato K, Ito H, Kamei K, Inaguma Y, Iwamoto I, Saga S. 1998. Phosphorylation of alphaB-crystallin in mitotic cells and identification of enzymatic activities responsible for phosphorylation. J Biol Chem. 273(43):28346–28354. doi:10.1074/jbc.273.43.28346.

Kato K, Ito H, Kamei K, Iwamoto I, Inaguma Y. 2002. Innervation-dependent phosphorylation and accumulation of alphaB-crystallin and Hsp27 as insoluble complexes in disused muscle. FASEB J. 16(11):1432–1434. doi:10.1096/fj.02-0129fje.

Koh HJ, Toyoda T, Fujii N, Jung MM, Rathod A, Middelbeek RJ-W, Lessard SJ, Treebak JT, Tsuchihara K, Esumi H, *et al.* 2010. Sucrose nonfermenting AMPK-related kinase (SNARK) mediates contraction-stimulated glucose transport in mouse skeletal muscle. Proc Natl Acad Sci U S A. 107(35):15541–15546. doi:10.1073/pnas.1008131107.

Kondo S, Ueda R. 2013. Highly improved gene targeting by germline-specific Cas9 expression in Drosophila. Genetics. 195(3):715–721. doi:10.1534/genetics.113.156737.

LaBeau-DiMenna EM, Clark KA, Bauman KD, Parker DS, Cripps RM, Geisbrecht ER. 2012. Thin, a Trim32 ortholog, is essential for myofibril stability and is required for the integrity of the costamere in Drosophila. Proc Natl Acad Sci U S A. 109(44):17983–17988. doi:10.1073/pnas.1208408109.

Li Y, Xie W, Fang G. 2008. Fluorescence detection techniques for protein kinase assay. Anal Bioanal Chem. 390(8):2049–2057. doi:10.1007/s00216-008-1986-z.

Lizcano JM, Göransson O, Toth R, Deak M, Morrice NA, Boudeau J, Hawley SA, Udd L, Mäkelä TP, Hardie DG, *et al.* 2004. LKB1 Is a master kinase that activates 13 kinases of the AMPK subfamily, including MARK/PAR-1. EMBO J. 23(4):833–843. doi:10.1038/sj.emboj.7600110.

Meharena HS, Fan X, Ahuja LG, Keshwani MM, McClendon CL, Chen AM, Adams JA, Taylor SS. 2016. Decoding the interactions regulating the active state mechanics of eukaryotic protein kinases. PLoS Biol. 14(11):e2000127. doi:10.1371/journal.pbio.2000127.

Molina E, Hong L, Chefetz I. 2021. NUAK kinases: brain-ovary axis. Cells. 10(10):2760. doi:10.3390/cells10102760.

Peschek J, Braun N, Franzmann TM, Georgalis Y, Haslbeck M, Weinkauf S, Buchner J. 2009. The eye lens chaperone alpha-crystallin forms defined globular assemblies. Proc Natl Acad Sci U S A. 106(32):13272–13277. doi:10.1073/pnas.0902651106.

Ranganayakulu G, Schulz RA, Olson EN. 1996. Wingless signaling induces nautilus expression in the ventral mesoderm of the Drosophila embryo. Dev Biol. 176(1):143–148. doi:10.1006/dbio.1996.9987.

Reece-Hoyes JS, Walhout AJM. 2018. Gateway recombinational cloning. Cold Spring Harb Protoc. 2018(1):pdb.top094912. doi:10.1101/pdb.top094912.

Reimann L, Wiese H, Leber Y, Schwäble AN, Fricke AL, Rohland A, Knapp B, Peikert CD, Drepper F, van der Ven PFM, *et al.* 2017. Myofibrillar Z-discs are a protein phosphorylation hot spot with protein kinase C (PKCα) modulating protein dynamics. Mol Cell Proteomics. 16(3):346–367. doi:10.1074/mcp.M116.065425.

Schiller NR, Duchesneau CD, Lane LS, Reedy AR, Manzon ER, Hoppe PE. 2017. The role of the UNC-82 protein kinase in organizing myosin filaments in striated muscle of *Caenorhabditis elegans*. Genetics. 205(3):1195–1213. doi:10.1534/genetics.116.193029.

Singh BN, Rao KS, Rao CM. 2010. Ubiquitin-proteasome-mediated degradation and synthesis of MyoD is modulated by alphaB-crystallin, a small heat shock protein, during muscle differentiation. Biochim Biophys Acta. 1803(2):288–299. doi:10.1016/j.bbamcr.2009.11.009.

Steinberg GR, Hardie DG. 2023. New insights into activation and function of the AMPK. Nat Rev Mol Cell Biol. 24(4):255–272. doi:10.1038/s41580-022-00547-x.

Sun X, Gao L, Chien HY, Li WC, Zhao J. 2013. The regulation and function of the NUAK family. J Mol Endocrinol. 51(2):R15–R22. doi:10.1530/JME-13-0063.

Suzuki A, Kusakai G, Kishimoto A, Lu J, Ogura T, Lavin MF, Esumi H. 2003. Identification of a novel protein kinase mediating akt survival signaling to the ATM protein. J Biol Chem. 278(1):48–53. doi:10.1074/jbc.M206025200.

Ueda Y, Duncan MK, David LL. 2002. Lens proteomics: the accumulation of crystallin modifications in the mouse lens with age. Invest Ophthalmol Vis Sci. 43:205–215.

van de Vis RAJ, Moustakas A, van der Heide LP. 2021. NUAK1 And NUAK2 fine-tune TGF-β signaling. Cancers (Basel). 13(13):3377. doi:10.3390/cancers13133377.

Wang X, Klevitsky R, Huang W, Glasford J, Li F, Robbins J. 2003. AlphaB-crystallin modulates protein aggregation of abnormal desmin. Circ Res. 93(10):998–1005. doi:10.1161/01.RES.0000102401.77712.ED.

Wójtowicz I, Jabłońska J, Zmojdzian M, Taghli-Lamallem O, Renaud Y, Junion G, Daczewska M, Huelsmann S, Jagla K, Jagla T. 2015. Drosophila Small heat shock protein CryAB ensures structural integrity of developing muscles, and proper muscle and heart performance. Development. 142(5):994–1005. doi:10.1242/dev.115352.

Xue L, Tao WA. 2013. Current technologies to identify protein kinase substrates in high throughput. Front Biol (Beijing). 8(2):216–227. doi:10.1007/s11515-013-1257-z.

Yamaguchi T, Arai H, Katayama N, Ishikawa T, Kikumoto K, Atomi Y. 2007. Age-related increase of insoluble, phosphorylated small heat shock proteins in human skeletal muscle. J Gerontol A Biol Sci Med Sci. 62(5):481–489. doi:10.1093/gerona/62.5.481.

Yamamoto H, Takashima S, Shintani Y, Yamazaki S, Seguchi O, Nakano A, Higo S, Kato H, Liao Y, Asano Y, *et al.* 2008. Identification of a novel substrate for TNFalpha-induced kinase NUAK2. Biochem Biophys Res Commun. 365(3):541–547. doi:10.1016/j.bbrc.2007.11.013.

Yeh YY, Wrasman K, Herman PK. 2010. Autophosphorylation within the Atg1 activation loop is required for both kinase activity and the induction of autophagy in Saccharomyces cerevisiae. Genetics. 185(3):871–882. doi:10.1534/genetics.110.116566.

Zagórska A, Deak M, Campbell DG, Banerjee S, Hirano M, Aizawa S, Prescott AR, Alessi DR. 2010. New roles for the LKB1-NUAK pathway in controlling myosin phosphatase complexes and cell adhesion. Sci Signal. 3(115):ra25. doi:10.1126/scisignal.2000616.

Editor: R. Duronio